JOURNAL OF AIRCRAFT
Vol. 34, No. 3, May–June 1997

Unsteady Pressure Measurements for Parallel Vortex–Airfoil Interaction at Low Speed

Jerry M. Chen* and Dar-Ming Chang†
National Chung-Hsing University, Taichung, Taiwan, Republic of China

Two-dimensional vortex–airfoil interaction at airfoil chord Reynolds number 6×10^4 is studied experimentally by immersing an instrumented NACA 0012 airfoil downstream of a vortex generator airfoil that pitches in a tailored nonsinusoidal form. A clockwise rotating vortex is generated to approach the target airfoil from left to right. When the vortex interacts with a nonlifting airfoil, it creates rather sharp and local variations of surface pressure in the vicinity of the leading edge. For airfoils at an angle of attack (α = 5 and 10 deg), the pressure variations appear to be spread over nearly the entire surface. Nevertheless, a greater magnitude in the amplitude of transient lift is noted on the airfoil at high angle of attack (α = 10 deg), primarily because of a low-pressure plateau region formed on the upper surface that occurs when the vortex moves downstream of the trailing edge. The amplitude of transient lift is also found to increase with a reduction in the vertical separation between the vortex generator and the airfoil.

Nomenclature

C = chord length of airfoil model
Cl = lift coefficient, $L/(\rho U_\infty^2 C/2)$
Cl_{max} = maximum lift coefficient
Cl_{min} = minimum lift coefficient
C_p = pressure coefficient, $(p - p_\infty)/(\rho U_\infty^2/2)$
L = lift
p = pressure
p_∞ = freestream static pressure
Re = Reynolds number, $U_\infty C/\nu$
t = time
U_c = vortex convection velocity
U_∞ = freestream velocity
u = horizontal velocity component
v = vertical velocity component
X_v = horizontal distance from quarter chord of vortex generator
x = axial distance from leading edge
Y_v = vertical separation between vortex generator and airfoil model
y = vertical distance from centerline of test section
α = angle of attack of airfoil model
Γ_v = vortex circulation
Γ_v^+ = dimensionless vortex circulation, $\Gamma_v/U_\infty C$
θ_p = angle of attack of vortex generator
ν = kinematic viscosity
ρ = fluid density
τ = dimensionless time, tU_∞/C
ω = spanwise vorticity
ω^+ = dimensionless vorticity, $\omega C/U_\infty$

Introduction

THE interaction of rotor blade with the incoming vortices shed from a proceeding blade has been recognized as a major source of noise and vibration in most helicopters and turbomachines. Similar interaction also occurs in the remotely piloted vehicles and modern fighter aircraft that are equipped with canard and wing. The vortical wake produced from the canard can significantly affect the aerodynamic characteristics of the downstream wing during high-angle-of-attack flight.[1,2]

The flow of vortex–airfoil interaction is a highly complex problem because it is generally three dimensional and time dependent in nature. A comprehensive theory reliably describing this complex flow behavior seems unavailable to date. Many of the analytical studies on this problem have focused on the two-dimensional (parallel) interaction that occurs when the axis of the vortex is parallel to the span of the airfoil. Saffman and Sheffield[3] and Huang and Chow[4] used the potential theory to obtain the unsteady lift and the stable trajectory of a vortex past an airfoil. Hsu and Wu[5] further considered the viscous effects caused by the approaching vortex on the airfoil surface to compute the unsteady lift. These analytical studies have indicated that the unsteady lift is a function of the vortex strength, the relative location of the vortex, and the angle of attack of the airfoil. Numerous details of the vortex–airfoil interaction have also been revealed by computational studies. A number of researchers[6–10] employed the vortex methods to investigate the evolution of the vortex structure during the interaction process. These two-dimensional simulations have been able to demonstrate the significance of vortex convection and deformation as well as the resultant aerodynamic loading of the airfoil. In particular, the use of a vortex cloud to represent the incoming vorticity field by Lee and Smith[8] has shown that the vortex of smaller size produces a distinct change in lift as it passes the airfoil trailing edge. Srinivasan and McCroskey,[11] who recently calculated the unsteady surface pressure of a rotor interacting with a line vortex using the three-dimensional Euler equations, have pointed out that the unsteady time-lag and three-dimensional effects may be negligible for subsonic flow while those effects become significant for transonic flow because of the oblique shock generated during the interaction.

Experiments on the two-dimensional vortex–airfoil interaction focus on conspicuous details of the problem and are useful to reveal fundamental mechanisms of the interaction. Booth and Yu[12] immersed a stationary airfoil behind another sinusoidally oscillating airfoil in a low-speed wind tunnel to observe the trajectory and deformation of the passing vortex during the interaction. Similar experimental setup was also employed by Poling and Telionis[13] and Poling et al.[14] in a water tunnel to examine the unsteady flowfield over the stationary airfoil. However, the discrete vortices generated by this means may be too close to detect the effects of individual vortices

Received April 20, 1996; revision received Jan. 7, 1997; accepted for publication Jan. 15, 1997.

*Associate Professor, Department of Mechanical Engineering. Member AIAA.
†Graduate Assistant, Department of Mechanical Engineering.

during the interaction. Seath et al.[15] and Straus et al.[16] later investigated the vortex–airfoil interaction by the use of an impulsively pitching wing that produced a starting vortex to interact with a downstream nonlifting airfoil. The pressure measurements of Seath et al.[15] have indicated that the airfoil surface pressure change near the leading edge increases as the maximum vortex generator pitch angle is increased from 10 to 20 deg. They have also pointed out that the starting vortex generated during the pitchup stroke may be accompanied by a dynamic stall vortex at higher pitch angles (15–20 deg). Note that the dynamic stall vortex rotates in a direction opposite to the starting vortex. Similarly, using impulsive pitching of airfoil, but with a much smaller pitch angle to produce a starting vortex, Swirydczuk[17] was able to perform smoke visualization of the vortex interacting with another downstream airfoil. Although details of the interaction between a well-defined free vortex and the airfoil were apparent in Swirydczuk's experiment,[17] the strength of the vortex was too weak to allow pressure measurements on the airfoil.

To compute the transient airfoil loading for low-speed vortex–airfoil interaction, Booth[18] utilized microphones to measure the temporal airfoil surface pressure around the forward 25% of the airfoil chord. The incoming vortex was generated by an upstream oscillating airfoil that pitched in a tailored nonsinusoidal form. This method permits good control and measurement of the vortex. However, the transient airfoil lift reported by Booth[18] exhibits multiple impulses (lobes of large fluctuations) during the interaction and it differs from other experimental and numerical simulations aforementioned. Experiments on the two-dimensional blade–vortex interaction at transonic speeds have been conducted by Meier and Timm[19] and Lee and Bershader[20] in a shock tube where vortices were generated by impulsive starting of the flow over an airfoil. In these experiments, flow visualization by interferometric techniques has shown substantial effects of viscosity during the interaction. In addition, a number of experiments[21–24] have been made to investigate the surface pressure and transient aerodynamic loads on a rotor blade of airfoil section that interacts with a vortex produced from an upstream wing tip. The interaction between the airfoil and vortex in such a manner is indeed three dimensional. However, some of the measurements with a limited rotor azimuth angle may be reasonably considered as a two-dimensional vortex–airfoil interaction. One such case was a recent experiment by Horner et al.,[24] who measured surface pressure distributions of a low-speed forwarding rotor blade interacting with an incoming vortex. Their results indicated discernible effects of interaction not only when the vortex approached the leading edge but also when it passed the trailing edge.

A review of the literature already cited indicates the complexity of the vortex–airfoil interaction increases from the linear subsonic regime to the nonlinear transonic regime. The interaction is benign under subsonic conditions. Therefore, favorable results such as transient pressure and loading on the airfoil are more accessible in the linear regime. The current work presents experimental data on the parallel vortex–airfoil interaction at very low speed. These experimental data may provide a source for validation of analytical/numerical modeling. One of the major difficulties involving this experiment is the generation of a well-defined isolated vortex normal to the flow velocity. The vortex generation technique employed by Booth[18] is adopted in the present investigation; a stationary airfoil model is immersed behind a vortex generator airfoil that pitches in a tailored nonsinusoidal form. This vortex generation technique not only permits good control of the vortex but also provides favorable accuracy of measurements when the data need ensemble averaging. Prior to the pressure measurements, the wake behind the vortex generator is surveyed to determine the strength and structure of the vortex. For the present experiment, a clockwise rotating vortex is generated to approach the airfoil model from left to right. For a loaded airfoil, i.e., an airfoil at an angle of attack, the orientation of the incoming vortex is opposite to that of many previous blade–vortex interaction experiments, however, such a vortex orientation often occurs in the wake vortex–airfoil interaction for typical carnard–wing configurations.[1,2] Unsteady pressure distributions on the airfoil model are measured and used to compute transient airfoil lift for two experimental parameters: 1) the angle of attack of the airfoil and 2) the vertical separation between the vortex generator and the airfoil.

Description of Experiment

The experiments were performed in a low-speed open-type wind tunnel with a square test section of 305 × 305 mm. The longitudinal turbulence level for the test velocity range was less than 0.5%. The experimental setup is shown schematically in Fig. 1. A test airfoil model of NACA 0012 profile with a 152-mm chord and 304-mm span was mounted horizontally about its quarter chord between the side plates of the test section. The airfoil model was immersed downstream of a vortex generator consisting of a 100-mm chord NACA 0012 airfoil with 303 mm in span. The vortex generator was directly driven by a servomotor about its quarter chord. The servomotor was controlled by an IBM AT compatible personal computer with a feedback control loop to ensure the assigned pitch schedule. An optical encoder coupled to the motor shaft was able to signify the transient angle of incidence of the vortex generator to an accuracy of 0.09 deg. The signal from the encoder was also used for the phase reference of measurements. The freestream was maintained at a constant velocity U_∞ = 6 m/s. The Reynolds number based on the test airfoil chord was $Re = 6 \times 10^4$. At this Reynolds number the boundary layer was likely laminar when the separation occurred.[10]

The unsteady surface pressure of the airfoil model was measured by a differential pressure transducer (ScanCo PDCR23D) installed in the Scanivalve system that was connected to the pressure ports on the airfoil surface with short tubes of equal length. There were 23 pressure ports on the airfoil model along its midspan surface. Twelve of the pressure ports were located at 0.5, 2.5, 7.5, 12.5, 20, 30, 40, 50, 60, 70, 80, and 90% chord on the upper surface. The remaining 11 pressure ports were located at 1, 5, 10, 15, 25, 35, 45, 55, 65, 75, and 85% chord on the lower surface. The natural frequency of the pressure transducer was higher than 35 kHz. Although the connection of the tubing to the transducer could considerably reduce the dynamic response, such an arrangement for pressure measurements was adequate for the present experiment.

A TSI anemometer system (IFA100) in conjunction with a cross hot-film probe was used to measure the velocity profiles. The probe was mounted on a two-dimensional traversing mechanism driven by stepper motors. The laboratory temperature was maintained at 21 ± 1°C during the course of each experiment.

The measurements of pressure and velocity were recorded by a multichannel analog data acquisition memory (ADAM

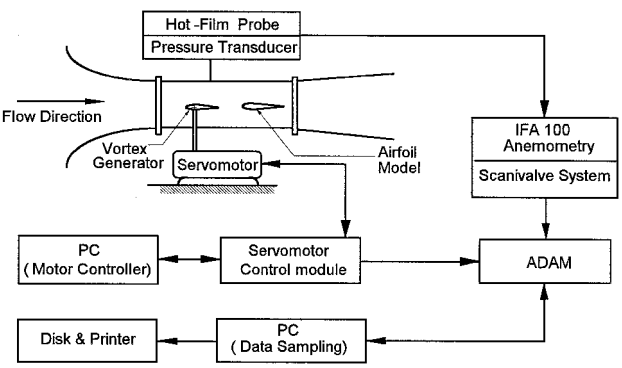

Fig. 1 Schematic of experimental setup.

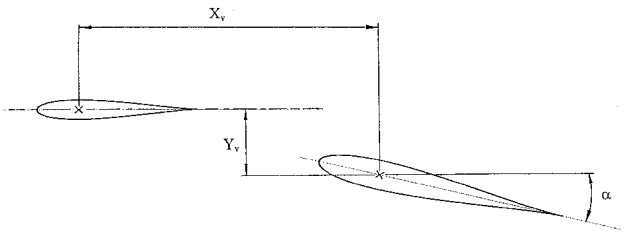

Fig. 2 Geometric parameters.

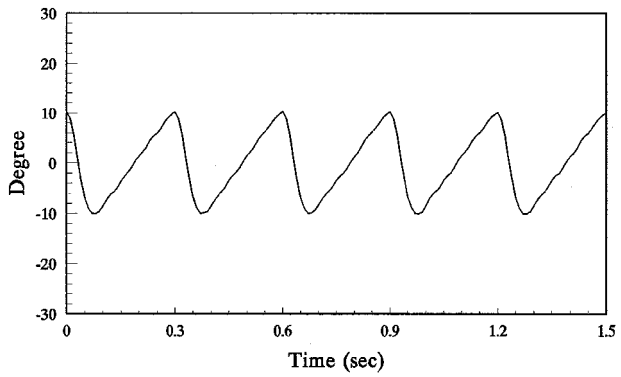

Fig. 3 Actual trajectory of the incidence angle of vortex generator. Uncertainty in incidence angle is ±0.09 deg.

ADC0512) that had individual A/D converters of 12 bit on each channel. The ADAM system was used mainly for the recording and displaying of sudden and transient signals.

Figure 2 shows the relative geometry of the two-dimensional vortex–airfoil interaction. The interaction was examined for the dimensionless vertical separation Y_v/C between -0.263 to $+0.263$. Y_v is positive when the vortex generator is situated above the airfoil model and negative when the vortex generator is below the airfoil model. The interaction was also examined for α between 0–10 deg. The horizontal distance X_v/C was set at 2.23 for the present experiment. In the worst case, the blockage ratio was 8.7% for the present experiment. No correction was made on the experimental results because of the blockage.

The vortex was produced by the vortex generator with a nonsinusoidal oscillation similar to that utilized by Booth.[18] The vortex generator was periodically oscillated between 10 and -10 deg about its quarter chord axis. The oscillation function was designed as follows:

$$\theta_p = \begin{cases} 10 \text{ deg} \cos(\pi t/0.072) & 0.0 \le t \le 0.075 \\ 25.526 \text{ deg}(t/0.3 - 0.60824) & 0.075 < t \le 0.3 \end{cases} \quad (1)$$

The actual trajectory executed by the vortex generator is depicted in Fig. 3. To create a region of concentrated vorticity, the first 25% of the oscillation schedule period was made by rapid sinusoidal pitchdown.[10] The vorticity generated during this pitchdown stroke was positive (clockwise). Then the vortex generator returned to 10 deg at a constant angular velocity and generated much weaker vorticity. The repeatability of the vortex generator motion was of vital importance to the present experiment because ensemble averaging was used to establish the results of unsteady pressure and velocity measurements. Repeated tests showed that the uncertainty in vortex generator position was within ±0.3 deg.

Flow visualization of the wake vortices behind the vortex generator was obtained using the smoke–wire technique. A thin wire was placed in the centerplane of the test section at 80 mm upstream of the vortex generator. The wire was heated at a voltage of 20–30 V. The visualized flowfield was illuminated by three lamps of 500 W. To compare with the velocity measurements, the flow visualization was conducted at the same flow speed $U_\infty = 6$ m/s.

It should be noted that the use of rather low aspect ratios of the airfoils was to obtain a high enough reduced pitch rate for the vortex generator and to provide a fine spatial resolution of pressure measurement for the airfoil model. These conditions demanded some compromise to be made with the flow two dimensionality. To check for three-dimensional effects, two additional pressure ports were located at ±6 cm from the midspan at a chordwise position $X/C = 0.2$ on the airfoil model. This chordwise position was chosen for the reason that pressure variations were pronounced only in the forward 20% chord length for most of the vortex–airfoil interaction cases presented. The maximum variation of C_p among the three different spanwise locations at $X/C = 0.2$ was found to be small (within ±4.5%), and therefore, sidewall interference may not significantly affect the pressure measurements along the midspan of the airfoil in the present investigation.

Results and Discussion

Vortex Structure

Figure 4 shows the smoke visualization of the wake behind the vortex generator. A well-defined, clockwise rotating vortex created during the rapid pitchdown stroke can be seen in the photograph. This well-defined vortex is followed by a train of smaller vortices. These smaller vortices are generated during the slower pitchup stroke.

Wake surveys were attempted to determine the strength of the vortex filament generated by the vortex generator using the tailored pitch schedule. A cross hot-film probe was traversed at a total of 40 points along a survey line position at the streamwise station where the leading edge of airfoil model is placed, i.e., $X_v/C = 2$. At each survey point the two-dimensional velocity was recorded for 80 oscillation cycles. This number of ensembles resulted in good convergence of the unsteady mean velocity profiles. The estimated uncertainty of the ensemble-averaged velocities u and v because of random errors was approximately ±5%. On the other hand the systematic error of the velocity measurements was about ±1.2%. Figure 5 shows u and v at $X_v/C = 2.0$ as functions of time. Note that the main nonzero portion of the perturbation velocity occurs in a short interval from $t = 0.075$ to 0.1 s, indicating the production of concentrated vorticity by this process. Moreover, ω was computed from the ensemble-averaged velocity data using the Taylor hypothesis to estimate the x derivative:

$$\omega = \frac{\partial u}{\partial y} - \frac{\partial v}{\partial x} \approx \frac{\partial u}{\partial y} + \frac{1}{U_c}\frac{\partial v}{\partial t} \quad (2)$$

The measured vortex convection velocity was approximately $0.99 \pm 0.01 U_\infty$. Thus, the freestream velocity was used as the

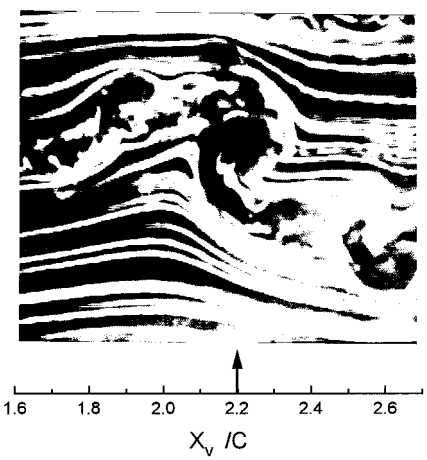

Fig. 4 Smoke visualization of the isolated vortex structure (arrow indicates the location of the vortex).

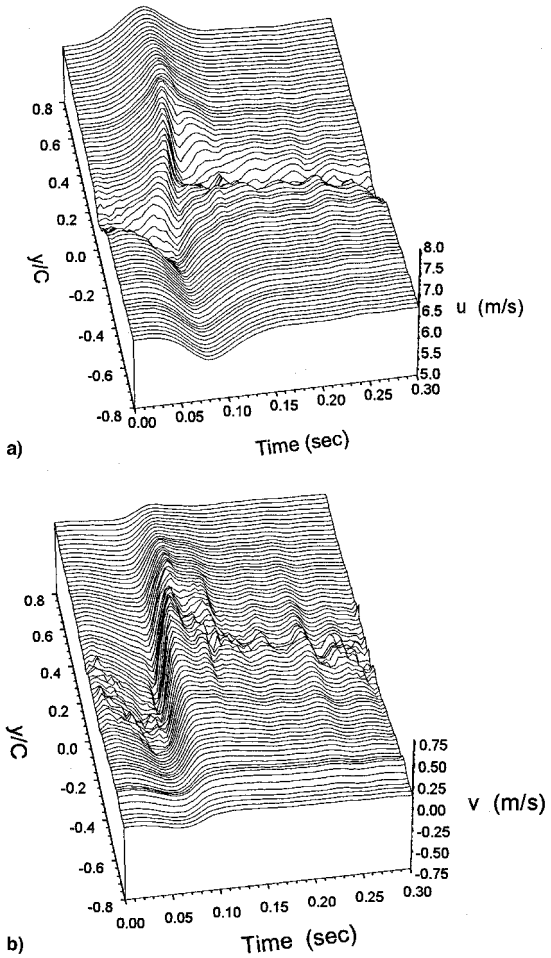

Fig. 5 Velocity time history of the tailored wake: a) u and b) v velocity profiles at X_v/C = 2.0. Uncertainty in both u and v is ±5.2%.

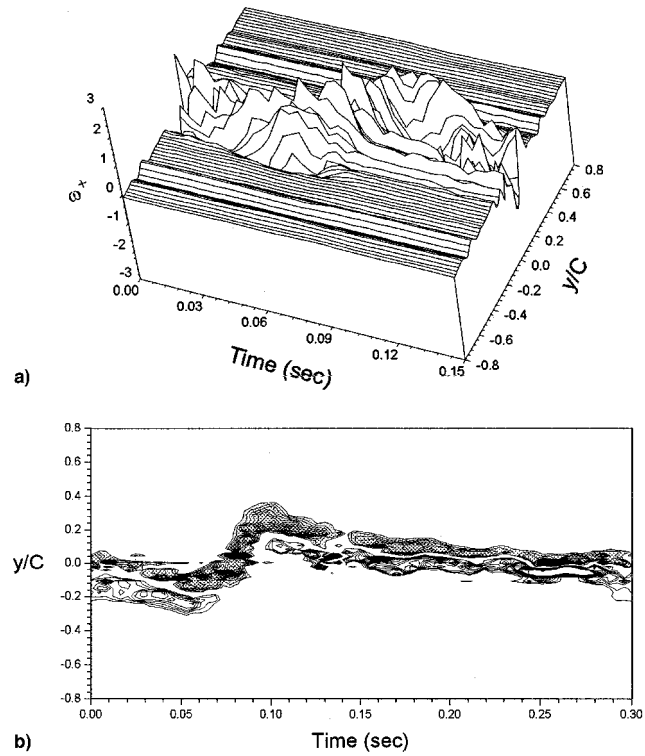

Fig. 6 Vorticity time history of the tailored wake. Vorticity a) field and b) contour, shaded area denotes positive vorticity. Uncertainty in ω^+ ranges from ±5 to ±18%.

convection velocity for the calculation of Eq. (2). To evaluate the derivatives in Eq. (2) the ensemble-averaged velocity data were fitted by cubic splines, and then the central differencing scheme was applied. Figure 6a presents ω^+, where $\omega^+ = \omega C/U_\infty$. The vorticity is defined as positive when the vortex is clockwise. Figure 6b is the nondimensional vorticity contour that demonstrates a region of relatively concentrated vorticity, i.e., some form of a vortex core as indicated in the flow visualization, in the interval time from t = 0.075 to 0.1 s. The vorticity field depicted in Fig. 6 also appears to contain vorticity stretching upstream and downstream of the core. It should be noted that the contour is rather a frozen field over a short distance than an instantaneous portrait of the vorticity distribution. The positive vorticity was further integrated over the survey line to obtain the vortex circulation Γ_v = 0.48 m^2/s, or in dimensionless form $\Gamma_v^+ = \Gamma_v/U_\infty C$ = 0.516. The uncertainty in the computed positive circulation from the velocity measurements may be estimated by comparing with the negative circulation generated in the pitchup stroke portion,[25] which was found to be 0.4 m^2/s. The total circulation in one cycle of oscillation must be zero, and so the error of the vortex circulation presented is about ±9%.

Surface Pressure

Measurements of surface pressure variations were used to examine the response of the airfoil model to the encountering vortex. To obtain the unsteady mean pressure distribution, the ensemble averaging was employed with 10 oscillation cycles at each pressure port. This number of ensembles not only produced good convergence of the unsteady mean but also reduced the fluctuations because of von Kármán vortices. It was found that the rms value of the fluctuations of C_p near the leading edge could be reduced from 0.04 to 0.006 after the ensemble averaging for the present experiment. The estimated uncertainty in C_p because of random errors was approximately ±3%. Figure 7 shows the pressure distributions as a function of nondimensional time $\tau = tU_\infty/C$ for three angles of attack α = 0, 5, and 10 deg. These data reflect the interaction with zero vertical separation between the vortex generator and the airfoil model, i.e., Y_v/C = 0. Note that τ also represents the streamwise location of the vortex in reference to the chord length with the assumption that the vortex travels at the freestream velocity and the minimum of the pressure on the lower surface occurred when the vortex center passed over it. When the vortex has not come into effect (τ = 0), the pressure distributions appear to resemble those of static airfoils immersed in an undisturbed stream. As the vortex approaches the airfoil, its clockwise circulation tends to decrease the local angle of attack by a downwash effect. The vortex-induced downwash causes an increase in the upper surface pressure and a decrease in the lower surface pressure. As the vortex arrives at the nose (τ = 2.83), the leading pressure on the upper surface reaches a maximum. For the cases of α = 5 and 10 deg, the rise of the leading-edge pressure results in the shift of the suction peak from the neighborhood of the leading edge to a more downstream position. It is found that the leading-edge pressure for the airfoil at α = 5 deg rises to a value even greater than the trailing-edge pressure by 0.1 in C_p. At the same time (τ = 2.83), on the lower surface occurs the minimum pressure. It is also observed on the lower surface pressure that the vortex-induced downwash effect seems to be weaker with an increase in the angle of attack. This is because the incoming clockwise vortex tends to unload rather than load the airfoil. Subsequently, as the vortex center passes over the leading edge of the airfoil, the upper surface pressure starts to descend while the lower surface pressure starts to rise. When the vortex con-

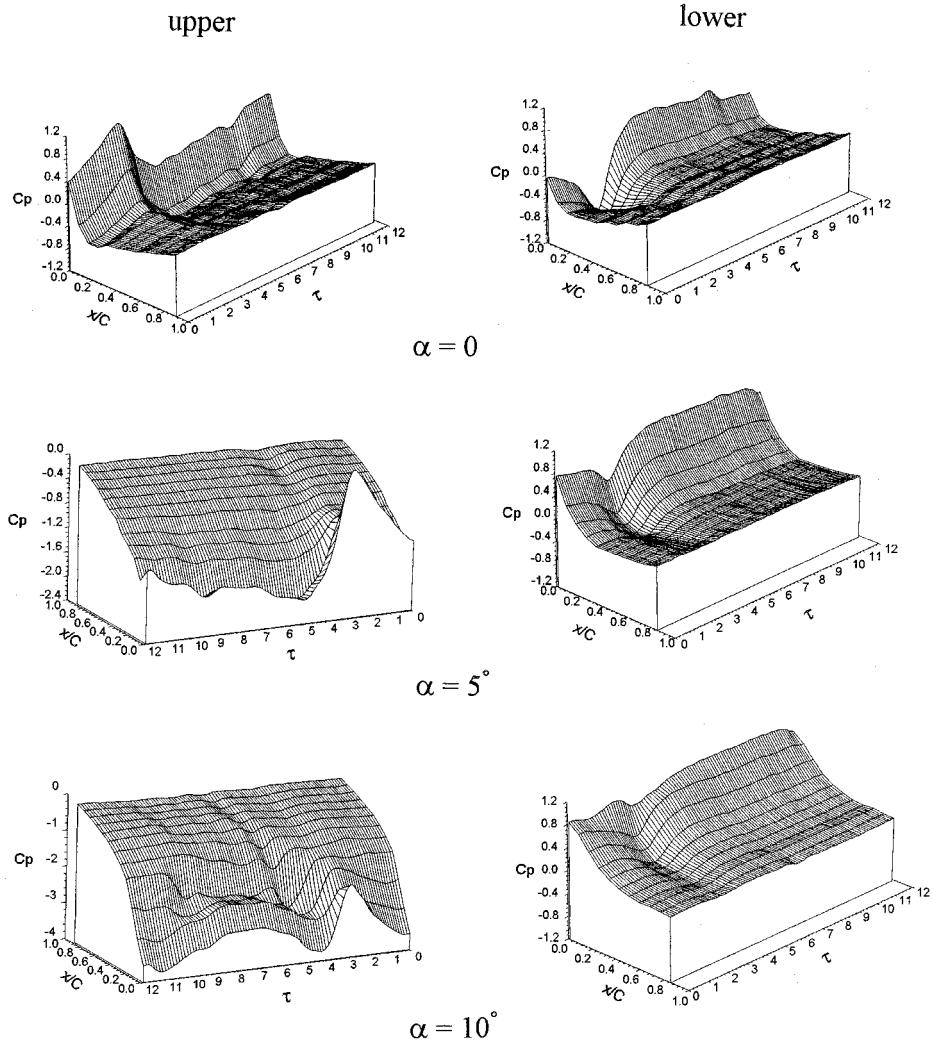

Fig. 7 Time history of chordwise pressure distributions on the upper and lower surfaces of the airfoil at α = 0, 5, and 10 deg for Y_c/C = 0. Uncertainty in C_p is ±3%.

vects to downstream of the trailing edge, the leading-edge pressure on the upper surface drops to a minimum value for all of the cases presented in Fig. 7. For the loaded airfoils (α = 5 and 10 deg), the suction peak on the upper surface now moves back to the leading edge, indicating an increase in local angle of attack. Meanwhile, the leading-edge pressure on the lower surface of the nonlifting airfoil ascends to a maximum (C_p = 0.4), meaning an upwash effect that changes the local angle of attack from positive to negative. For the loaded airfoils the lower surface pressure variations are not as sharp as the nonlifting airfoil but are spread more over the entire surface. As the vortex moves far downstream, the surface pressure then returns to an assumed steady case. During this stage pressure fluctuations can be observed, but are of smaller magnitude compared with the disturbance of the approaching vortex. The fluctuations are because of the unsteadiness of the wake produced by the upstream vortex generator during a relatively slow pitchup stroke.

The observation of Fig. 7 indicates that the tailored pitching oscillation of the vortex generator creates a distinct alteration in the airfoil pressure distribution during the vortex–airfoil interaction. For the nonlifting airfoil, this vortex-induced alteration is dominated in the 20–30% chord from the leading edge, this is consistent with the observation of Booth.[18] However, for the airfoil at α = 5 and 10 deg, the disturbance on the pressure distribution because of the approaching vortex extends more downstream on the upper surface and appears to be spread over the entire lower surface. Furthermore, in the case of α = 10 deg, a rather flat plateau region occurs on the upper surface distribution immediately downstream of the leading edge (X/C = 0.025–0.125) at about τ = 4.5. This low-pressure plateau may be indicative of the formation of a separation bubble.[26] The development and collapse of the low-pressure plateau may cause the surface pressure fluctuation stretching out to the trailing edge. In our flow visualization experiment the smoke was not dense enough at this freestream speed to allow clear observation of the formation of the separation bubble. Good photographs depicting a similar formation of the separation bubble can be found in the water-tunnel experiment by Shih and Ho.[27] The variation of the pressure distribution also exhibits that the vortex-induced alteration starts when the vortex moves to approximately a chord length upstream of the leading edge and ends when the vortex convects to about two chord lengths downstream of the trailing edge of the airfoil model. This is similar to the observation of Seath et al.[15]

Lift Coefficients

The unsteady lift can be obtained by the integration of chordwise pressure distributions. The estimated uncertainty in lift coefficient because of random errors was about ±5% of the maximum value. Figure 8 shows the variation of lift coefficient with nondimensional time for α = 0, 5, and 10 deg and for the vertical separation spacing between Y_c/C = −0.263 to 0.263. All of these cases exhibit a similar impulse of lift variation during the interaction process. As the positive (clock-

wise) vortex approaches the leading edge, the airfoil experiences a downwash effect, resulting in a decrease in lift coefficient. As the vortex reaches the nose of the airfoil ($\tau = 2.83$), the lift coefficient falls to a minimum for all of the cases presented. Subsequently, as the vortex center passes over the airfoil, the lift coefficient rises more rapidly than it falls. When the vortex leaves the airfoil ($\tau = 4.83$), the lift coefficient reaches a maximum. Thereafter, the lift coefficient decreases gradually and eventually approaches an assumed steady state. The rate of decrease seems more rapid at higher angles of attack. During the interaction, multiple impulses observed by Booth[18] in his measurements of transient lift are not found in our cases. Instead, only a single impulse is observed in Fig. 8. The appearance of a second impulse in Booth's experiment[18] could be because using microphones and long tubing for his measurements resulted in questionable time accuracy.[28] Nevertheless, the variations of the transient lift amplitude with the vortex generator position and the airfoil incidence are nearly quantitatively consistent between the presented results and Booth's results.[18] When we compare our results with the numerical calculations of Lee and Smith,[8] the agreement is good

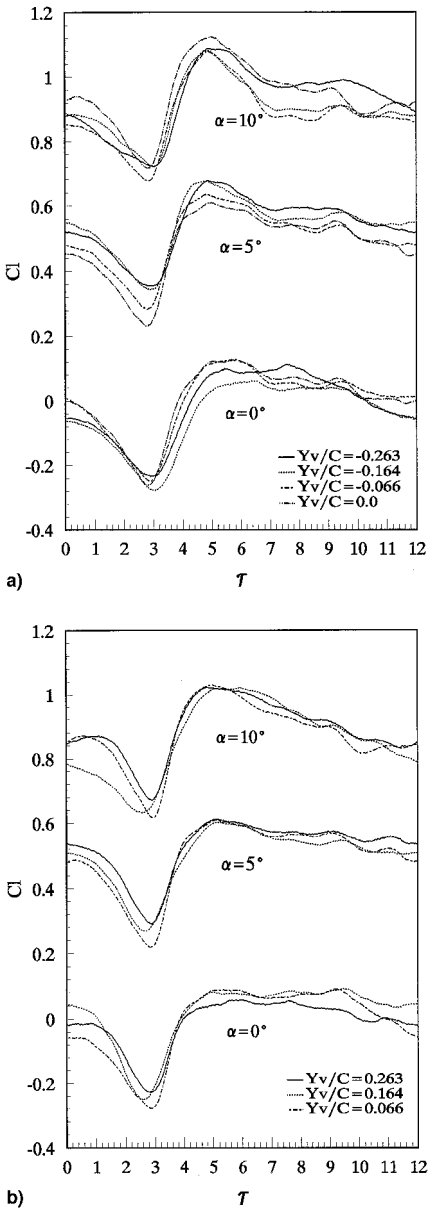

Fig. 8 Unsteady lift coefficients of the airfoil at different angles of attack. Y_v/C = a) −0.263–0 and b) 0.066–0.263. Uncertainty in Cl is ±0.017.

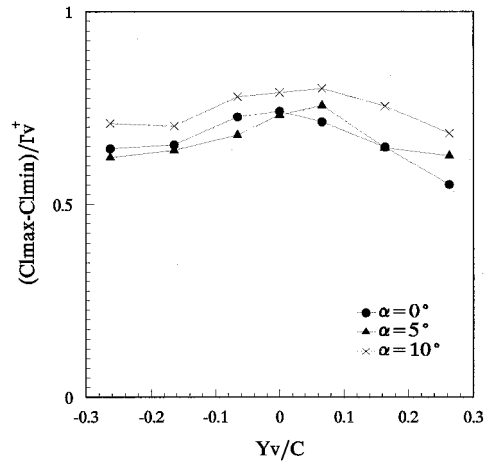

Fig. 9 Comparison of $(Cl_{max} - Cl_{min})/\Gamma_v^+$ vs Y_v/C for different angles of attack. Uncertainty in $(Cl_{max} - Cl_{min})/\Gamma_v^+$ is ±10.3%.

on the trend in the transient lift, except that the amplitudes of transient lift in the cases presented previously are smaller than the numerical results.

The difference between the maximum and minimum lift coefficients $(Cl_{max} - Cl_{min})/\Gamma_v^+$ vs vertical separation of the vortex generator and the airfoil Y_v/C is presented in Fig. 9. It shows that the influence on the lift coefficient is enhanced by adjusting the vortex generator toward smaller vertical separation with respect to the airfoil model, i.e., smaller $|Y_v/C|$. This trend agrees with the experimental results of Horner et al.,[24] but the magnitude of $(Cl_{max} - Cl_{min})/\Gamma_v^+$ obtained in the present experiment is about half of theirs. This discrepancy may be because the vortex circulation computed for the present experiment is an accumulation of the positive vorticity produced during the entire oscillation period of the vortex generator rather than an integration over the short interval that produces the concentrated region of vorticity. This figure also shows that the lift coefficient difference for $\alpha = 10$ deg is larger than that for $\alpha = 0$ and 5 deg by about 15%. This difference may be attributed to the flat plateau region of low pressure formed on the upper surface of the airfoil at $\alpha = 10$ deg near the end of the interaction. Although the vortex-induced disturbance is more spread over the entire lower surface pressure distribution for higher angles of attack, the formation and collapse of the low-pressure plateau on the upper surface may cause the lift to fall more quickly for $\alpha = 10$ deg than that for $\alpha = 0$ and 5 deg.

Conclusions

Two-dimensional vortex–airfoil interaction at low speed has been studied experimentally by immersing an airfoil model downstream of a vortex generator airfoil that pitches in a tailored nonsinusoidal form. Both flow visualization and wake surveys at the same flow speed show a region of relatively concentrated vorticity produced by the vortex generator.

Detailed pressure measurements taken about the upper and lower surfaces of the airfoil have revealed a distinct alteration in pressure distribution during the interaction of the vortex with the airfoil. As the clockwise vortex approaches the airfoil from left to right, the vortex tends to decrease the local angle of attack causing the upper surface pressure to rise and the lower surface to drop. When the vortex leaves the airfoil the pressure variation is opposite. The disturbance of the approaching vortex on the pressure distribution is rather sharp and limited in the forward 20–30% chord for a nonlifting airfoil ($\alpha = 0$). However, for loaded airfoils ($\alpha = 5$ and 10 deg), the disturbance extends more downstream on the upper surface and appears to be spread over the entire lower surface. The unsteady airfoil lift varies as a single impulse form in accordance with the location of the vortex. The approaching vortex

has a downwash effect on the airfoil, resulting in a reduction of lift, whereas the departure of the vortex causes an increase in lift (upwash). It is found that the amplitude of the transient lift for the airfoil at $\alpha = 10$ deg is larger than that at $\alpha = 0$ and 5 deg by about 15%, primarily because of a flat plateau region of low pressure formed in the vicinity of the leading edge of the airfoil at $\alpha = 10$ deg near the end of the interaction. It is also found that the amplitude of the transient lift is increased by a reduction in the vertical separation between the vortex generator and the airfoil.

Acknowledgments

Financial support for this research from the National Science Council of the Republic of China under Contracts NSC 85-2212-E-005-021 and NSC 86-2612-E-005-001 is gratefully acknowledged.

References

[1]Michelsen, W. D., and Mueller, T. J., "Low Reynolds Number Airfoil Performance Subjected to Wake Interference from an Upstream Airfoil," AIAA Paper 87-2351, Aug. 1987.

[2]Khan, F. A., and Mueller, T. J., "Tip Vortex/Airfoil Interaction for a Low Reynolds Number Carnard/Wing Configuration," *Journal of Aircraft*, Vol. 28, No. 3, 1991, pp. 181–186.

[3]Saffman, P. G., and Sheffield, J. S., "Flow over a Wing with an Attached Free Vortex," *Studies in Applied Mathematics*, Vol. 57, 1977, pp. 107–117.

[4]Huang, M. K., and Chow, C. Y., "Trapping of a Free Vortex by Joukowski Airfoils," *AIAA Journal*, Vol. 20, No. 3, 1982, pp. 292–298.

[5]Hsu, A. T., and Wu, J. C., "Vortex Flow Model for the Blade-Vortex Interaction Problem," *AIAA Journal*, Vol. 26, No. 5, 1988, pp. 621–623.

[6]Panaras, A. G., "Numerical Modeling of the Vortex/Airfoil Interaction," *AIAA Journal*, Vol. 25, No. 1, 1987, pp. 5–11.

[7]Poling, D. R., Dadone, L., and Telionis, D. P., "Blade-Vortex Interaction," *AIAA Journal*, Vol. 27, No. 6, 1989, pp. 694–699.

[8]Lee, D. J., and Smith, C. A., "Effect of Vortex Core Distortion on Blade-Vortex Interaction," *AIAA Journal*, Vol. 29, No. 9, 1991, pp. 1355–1362.

[9]Renzoni, P., and Mayle, R. E., "Incremental Force and Moment Coefficients for Parallel Blade-Vortex Interaction," *AIAA Journal*, Vol. 29, No. 1, 1991, pp. 6–13.

[10]Mook, D. T., and Dong, B., "Perspective: Numerical Simulation of Wakes and Blade-Vortex Interaction," *Journal of Fluids Engineering*, Vol. 116, No. 1, 1994, pp. 5–21.

[11]Srinivasan, G. R., and McCroskey, W. J., "Euler Calculations of Unsteady Interaction of Advancing Rotor with a Line Vortex," *AIAA Journal*, Vol. 31, No. 9, 1993, pp. 1659–1666.

[12]Booth, E. R., Jr., and Yu, J. C., "Two-Dimensional Blade-Vortex Flow Visualization Investigation," *AIAA Journal*, Vol. 24, No. 9, 1986, pp. 1468–1473.

[13]Poling, D. R., and Telionis, D. P., "The Response of Airfoils to Periodic Disturbances—The Unsteady Kutta Condition," *AIAA Journal*, Vol. 24, No. 2, 1986, pp. 193–199.

[14]Poling, D. R., Wilder, M. C., and Telionis, D. P., "Two-Dimensional Interaction of Vortices with a Blade," AIAA Paper 88-0044, Nov. 1988.

[15]Seath, D. D., Kim, J.-M., and Wilson, D. R., "Investigation of the Parallel Blade-Vortex Interaction at Low Speed," *Journal of Aircraft*, Vol. 26, No. 4, 1989, pp. 328–333.

[16]Straus, J., Renzoni, P., and Mayle, R. E., "Airfoil Pressure Measurements During a Blade-Vortex Interaction and a Comparison with Theory," *AIAA Journal*, Vol. 28, No. 2, 1990, pp. 222–228.

[17]Swirydczuk, J., "A Visualization Study of the Interaction of a Free Vortex with the Wake Behind an Airfoil," *Experiments in Fluids*, Vol. 9, No. 4, 1990, pp. 181–190.

[18]Booth, E. R., Jr., "Experimental Observation of Two-Dimensional Blade-Vortex Interaction," *AIAA Journal*, Vol. 28, No. 8, 1990, pp. 1353–1359.

[19]Meier, G. E. A., and Timm, R., "Unsteady Vortex Airfoil Interaction," CP-386, AD-P005-020, AGARD, May 1985.

[20]Lee, S., and Bershader, D., "Head-On Parallel Blade-Vortex Interaction," *AIAA Journal*, Vol. 32, No. 1, 1994, pp. 16–32.

[21]Caradonna, F. X., Laub, G. H., and Tung, C., "An Experimental Investigation of the Parallel Blade-Vortex Interaction," *Proceedings of the 10th European Rotorcraft Forum* (The Hague, The Netherlands), 1984.

[22]Caradonna, F. X., Strawn, R. C., and Bridgeman, J. O., "An Experimental and Computational Study of Rotor-Vortex Interaction," *Vertica*, Vol. 12, No. 4, 1988, pp. 315–327.

[23]Caradonna, F. X., Lautenschlager, J., and Silva, M., "An Experimental Study of Rotor-Vortex Interactions," AIAA Paper 88-0045, Jan. 1988.

[24]Horner, M. B., Saliveros, E., Kokkalis, A., and Galbraith, R. A. M., "Results from a Set of Low Speed Blade-Vortex Interaction Experiments," *Experiments in Fluids*, Vol. 14, No. 5, 1993, pp. 341–352.

[25]Panda, J., and Zaman, K. B. M. Q., "Experimental Investigation of the Flow Field of an Oscillating Airfoil and Estimation of Lift from Wake Surveys," *Journal of Fluid Mechanics*, Vol. 265, 1994, pp. 65–95.

[26]Ota, T., and Itasaka, M., "A Separated and Reattached Flow on a Blunt Flat Plate," *Journal of Fluids Engineering*, Vol. 98, No. 8, 1976, pp. 79–86.

[27]Shih, C., and Ho, C. M., "Vorticity Balance and Time Scales of a Two-Dimensional Airfoil in an Unsteady Free Stream," *Physics of Fluids*, Vol. 6, No. 2, 1994, pp. 710–723.

[28]Kalkhoran, I. M., and Wilson, D. R., "Experimental Investigation of the Parallel Vortex-Airfoil Interaction at Transonic Speeds," *AIAA Journal*, Vol. 30, No. 8, 1992, pp. 2087–2092.